J Solid State Electrochem (2003) 7: 134–140
DOI 10.1007/s10008-002-0295-2

ORIGINAL PAPER

W.T. Tan · E.B. Lim · A.M. Bond

Voltammetric studies on microcrystalline C_{60} adhered to an electrode surface by solvent casting and mechanical transfer methods

Received: 28 January 2002 / Accepted: 24 May 2002 / Published online: 22 August 2002

Abstract Voltammetric studies on C_{60} fullerene particles adhered to an electrode surface by solvent casting or mechanical transfer exhibit evidence of nucleation and growth controlled processes for the $C_{60}^{0/-}$ and $C_{60}^{-/2-}$ solid state when the modified electrode is in contact with acetonitrile solutions containing NBu_4^+ electrolyte. Although peak potentials and peak separations are dependent on scan rate as well as the amount of deposit and temperature, potentials obtained using a zero-current extrapolation method are almost independent of all these parameters. These data enable reversible potentials of –816 and –1168 mV vs. Ag/Ag^+ to be obtained in acetonitrile (0.1 M NBu_4PF_6) respectively for the processes: $C_{60}(solid) + NBu_4^+(solution) + e^- \rightleftharpoons NBu_4C_{60}(solid)$ and $NBu_4C_{60}(solid) + NBu_4^+(solution) + e^- \rightleftharpoons (NBu_4)_2C_{60}(solid)$. Images obtained by scanning electron microscopy reveal that both the crystalline and particle size is enhanced by 60 s of reductive electrolysis, with the detected $(NBu_4)_2C_{60}$ crystals being slightly larger than those of $(NBu_4)C_{60}$. After a short period of potential cycling or controlled potential electrolysis, it is concluded that the data obtained by either method of surface adherence are almost indistinguishable, as are their morphologies.

Keywords C_{60} · Fullerene · Solvent casting · Mechanical transfer · Voltammetry

Introduction

The properties of C_{60} fullerene have been widely investigated. For example, doped fullerene, which exhibits superconductivity [1, 2, 3] or ferromagnetism [4, 5], has found importance in application as a superconductor, photoelectrochemical sensor [6] and conducting polymer [7, 8]. Electrochemical studies of fullerene, which are of interest in this study, are also widespread. Early studies of dissolved fullerene in non-polar solvents [9], polar solvents [10] or mixed solvents [11, 12] indicated the presence of up to six reversible one-electron reduction steps. Solid fullerene, attached to an electrode surface mechanically or via solvent casting [13, 14, 15, 16, 17, 18, 19, 20], sublimation [21], electro-deposition [22, 23] or vapor deposition [24] methods, exhibits significantly different electrochemical behavior from that observed when C_{60} is dissolved in solution. In the case of cyclic voltammetry of solid fullerene adhered to an electrode in contact with acetonitrile containing a NBu_4^+ salt as the electrolyte, one of the most interesting aspects is the large peak separation and very narrow peak width of some of the processes [13, 14, 15, 16, 17]. Simultaneous cyclic voltammetry and electrochemical quartz crystal microbalance [25, 26] studies as well as microscopy [16] studies provided evidence that mass changes, dissolution of fullerene salts, and resistivity changes accompany reduction-reoxidation processes, and also revealed that structural rearrangements or reconstruction of solids is consequent upon the uptake or intercalation of NBu_4^+ into the fullerene lattice layer upon reduction.

In initial solid state studies, fullerene prepared by solvent casting or sublimation was attached to the electrode to give both thin and thick fullerene "films". From images obtained by atomic force microscopy and scanning electron microscopy (SEM) [13, 21], the surface structure of this "film" was shown to be irregular, consisting of crystallites of random size and orientation, which implies that the term "film" may be inappropriate under some circumstances and that the exact nature of the adhered solid may be critical to achieving an understanding of the voltammetry. Consequently, in this work, a detailed study of the electrochemistry using C_{60} layers made by both mechanical transfer of

W.T. Tan (✉) · E.B. Lim
Department of Chemistry, Universiti Putra Malaysia,
43400 UPM, Serdang, Selangor D.E., Malaysia
E-mail: wttan@fsas.upm.edu.my
Fax: +603-89432508

A.M. Bond
School of Chemistry, Monash University,
PO Box 23, Victoria 3800, Australia

microcrystals or solvent casting deposition techniques has been undertaken to further assess the effect of the various experimental parameters on the $C_{60}^{0/-}$ and $C_{60}^{-/2-}$ processes. The study extends some aspects of the knowledge generated in related studies described by Suàrez et al. [13], where evidence of a nucleation-growth process was detected for the $C_{60}^{0/-}$ process.

Experimental

Reagents

C_{60} (Fluka, 98%), quaternary ammonium salts, NR_4^+, such as NBu_4PF_6 (Merck), NBu_4BF_4 (Merck), NBu_4Cl (Fluka) and NBu_4ClO_4 (Sigma), were used as received. Analytical reagent grade solvents used were acetonitrile (Carlo Erba) and dichloromethane (BDH). Molecular sieves were added to the solvents to reduce the water content.

Preparation of electrodes

For the solvent casting experiments, C_{60} was deposited on a 1.6 mm diameter gold electrode (Bioanalytical System, USA). Initially, the electrode surface was polished, rinsed with relevant solvent, dried and finally coated with 20 μL (unless otherwise stated) of a 0.15 mM C_{60} dichloromethane (CH_2Cl_2) solution. Evaporation of the dichloromethane solvent produced a C_{60} chemically modified electrode. For the mechanical/abrasive attachment method, a small amount (1–3 mg) of C_{60} in microcrystalline form was spread onto a coarse grade filter paper and solid was transferred by gently rubbing the electrode surface onto the C_{60} coated filter paper.

Electrochemical measurements

A CV-50W electrochemical analyzer (Bioanalytical Sysytems, West Lafayette, Ind., USA) was used for the voltammetric experiments. A single-compartment, glass three-electrode electrochemical cell was used with a platinum wire as the counter electrode, and a Ag/Ag^+ (1 mM $AgNO_3$, 0.1 M NBu_4PF_6 in acetonitrile) reference electrode was placed near to the working electrode. The solutions were routinely deaerated with oxygen-free nitrogen gas for at least 10 min before each voltammetric measurement.

It is noted that a variability of ±10–20 mV in peak potentials obtained over the duration of this work was encountered. Data presented in the tables are normalized to one data set to minimize this problem.

Scanning electron microscopy

A piece of basal plane pyrolitic graphite (BPPG) (Alpha, USA) electrode with a 5 mm diameter and 2–3 mm thickness was cut from a rod. It was then polished with 320CW silicon carbide abrasive paper, followed by a further polishing with α-alumina (>99.5% Al_2O_3) powder. Similar methods of cleansing and deposition of microcrystals of C_{60} mentioned above for the gold surface were applied to the BPPG electrode experiments. To study the surface morphology of C_{60} on a BPPG electrode after electrolysis, the electrode, with an array of C_{60} microcrystals attached on the surface, was joined to a platinum wire that acted as a conductor. The reduction potential was then held at –1.800 V for 1 min in an appropriate electrolyte, using the bulk electrolysis mode of the electrochemical workstation (model BAS 100W). A scanning electron microscope, model JEOL JSM-6400 (Philips), was used to study the surface morphology of C_{60} before and after electrolysis.

Results

Effect of potential cycling

C_{60} coated onto an electrode surface by the solvent casting method provides significantly more stable voltammetry, particularly in the early stages of a potential cycling experiment, than when microcrystalline C_{60} is mechanically attached onto the electrode surface. Figure 1 shows the initial potential cycles for the $C_{60}^{0/-/2-}$ and $C_{60}^{-/2-}$ processes of cyclic voltammetry when C_{60} is coated by this method onto a 1 mm diameter gold electrode surface which is then placed in contact with acetonitrile (0.1 M NBu_4PF_6). Clearly the first cycle is distinctly different from all subsequent cycles. Whilst upon repetitive cycling the peak heights for the first and second reduction-reoxidation couples, designated processes I^{red}, II^{red}, II^{ox} and I^{ox}, decrease slightly, detailed analysis of data contained in Fig. 1 reveals that process I^{red} increases slightly for three cycles and decreases thereafter (peak height is 42 μA in the 10th cycle and 31 μA after the 40th cycle). The initial instability is attributable to a rearrangement in structure which improves the uniformity and accessibility of the C_{60} compound [15], while the minor decrease in extensive cycling of the potential is attributed to a small amount of dissolution of reduced C_{60}. After about three cycles of the potential, data detected by mechanical transfer of solid were very similar to those obtained with the solvent casting method. Minor processes detected between reactions I and II have been attributed to a slight solubility of some of the reduced microcrystals [15].

Effect of varying the amount of C_{60} adhered to the electrode surface

Based on analysis of the third cycle of the potential under conditions of Fig. 1, the peak current for process I^{ox} was

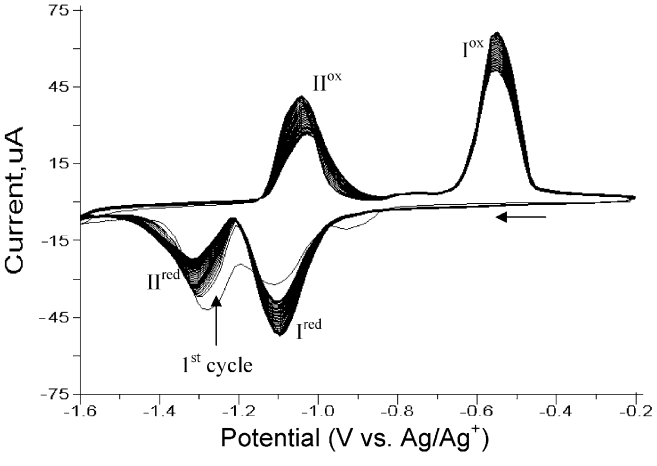

Fig. 1 First 40 cycles of a voltammogram obtained with a scan rate of 100 mV/s when 20 μL of 150 μM C_{60} (in CH_2Cl_2) was solvent cast onto a 1 mm gold electrode and the $C_{60}^{0/-/2-}$ processes was studied in MeCN (0.1 M NBu_4PF_6) over the potential range of –200 mV to –1600 mV (vs. Ag/Ag^+)

found to increase linearly as the amount of C_{60} solvent cast onto the electrode was varied from 10 to 60 μL of 0.150 mM C_{60} (Fig. 2). At higher amounts, non-linearity was observed. A smaller linear range was found for process I^{red} (Fig. 2). It is assumed that only partial electrolysis occurs on the time scale of the voltammetry, with very high surface coverage. The peak separation, ΔE_p, for process I also increased with increasing addition of C_{60} (Table 1), probably because of an enhanced IR_u (I = current, R_u = uncompensated resistance) drop. However, the potential measured as the average of E_p^{ox} and E_p^{red} is almost independent of the amount of C_{60}, as expected if it represents a formal $\left(E_f^\circ\right)$ reversible potential (Table 1) for the processes described in Eqs. 1 and 2:

$$C_{60}(\text{solid}) + NBu_4^+(\text{solution}) + e^- \rightleftharpoons NBu_4C_{60}(\text{solid}) \quad (1)$$

$$NBu_4C_{60}(\text{solid}) + NBu_4^+ + (\text{solution}) \rightleftharpoons (NBu_4)_2C_{60}(\text{solid}) \quad (2)$$

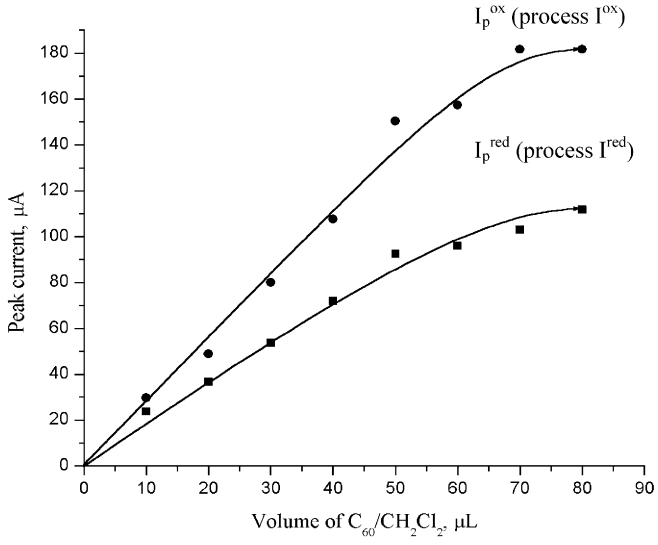

Fig. 2 Dependence of the peak currents for processes I^{red} and I^{ox} on the amount of C_{60} solvent cast onto a 1 mm gold electrode surface which is in contact with MeCN (0.1 M NBu_4PF_6). Data obtained for the third cycle of potential using parameters shown in Fig. 1

Scan reversal study

Previous studies [13, 14] have shown that intercalation of the R_4N^+ cation into the C_{60} lattice layer is not associated with a diffusion-controlled rate-determining step or "thin film" voltammetry. In particular, a nucleation-growth process [13] was detected for the $C_{60}^{0/-}$ process. One method that is diagnostic of a nucleation and growth process is the detection of current maxima when the potential is reversed [27, 28], before intercrystal collisions occur.

Cyclic voltammograms for C_{60} show a current maximum when the potential is switched prior to the peak potential for both the first and second redox processes (Fig. 3a, b). Evidence for a nucleation-growth process was much easier to obtain for the oxidation steps than for the reduction steps. The evidence provided in Suàrez et al. [13] for a nucleation and growth process for the $C_{60}^{0/-}$ process has now been extended to the $C_{60}^{-/2-}$ process. Evidence for the nucleation and growth process was obtained from both solvent cast and mechanical transfer C_{60} experiments. It may be assumed that the critical overpotential for conversion of C_{60}(solid) to $(NBu_4)C_{60}$(solid) has the same magnitude as for the reverse process, in order that the average value of the two peak potentials E_p^{red} and E_p^{ox} is equal to $\left(E_f^\circ\right)$ for process 1 (Eq. 1), with an analogous argument applying for process 2 (Eq. 2).

Scan rate study

Figure 4 shows the effect of varying the scan rate for the $C_{60}^{0/-}$ process using both C_{60} adherence methods. Generally, the current increases and the peak separation increases with scan rate for both coating methods. The nature of the scan rate dependence is consistent with a nucleation-growth mechanism (and/or uncompensated resistance). However, both coating techniques gave the zero-current extrapolated E_p^{red} potential at -1035 ± 19 mV and E_p^{ox} at -588 ± 7 mV for a wide range of samples (see Fig. 4c, for example). The result implies that the zero-current extrapolated potential is independent of the sample amount. The $\left(E_f^\circ\right)$ value calculated

Table 1 Potential data obtained for process I when C_{60}/CH_2Cl_2 is coated onto a 1 mm diameter gold electrode via the solvent casting method using specified volumes of a 0.15 mM C_{60} solution, and with the electrode being in contact with MeCN (0.1 M NBu_4PF_6). Data obtained from the third potential cycle using the conditions reported in Fig. 1

C_{60} volume (μL)	Red. peak potential, E_p^{red} (mV)	Ox. peak potential, E_p^{ox} (mV)	Peak separation, ΔE_p	Reversible potential, E_f° (mV)[a]
10	–1070	–551	519	–811
20	–1081	–550	531	–816
30	–1085	–542	543	–814
40	–1089	–538	551	–814
50	–1097	–526	571	–812
60	–1105	–526	579	–816
70	–1116	–513	603	–815
80	–1128	–513	615	–821

[a]Calculated as $\left(E_p^{red} + E_p^{ox}\right)/2$

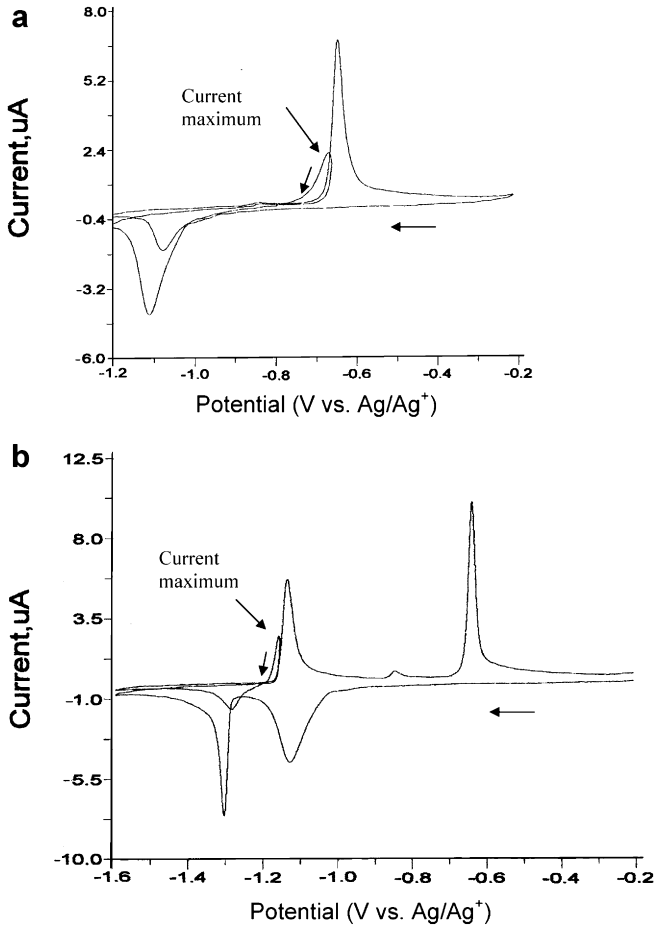

Fig. 3 **a** Detection of a current maximum for the first oxidation process when the direction of potential on the reverse scan is switched at the foot of process I^{ox}. The experiments were undertaken at a scan rate of 20 mV/s in MeCN (0.1 M NBu_4PF_6) using a 1 mm diameter gold electrode solvent cast with 10 μL of 0.15 mM C_{60}/CH_2Cl_2. The potential was initially swept from –200 mV to –1200 mV (vs. Ag/Ag^+). **b** Detection of a current maximum peak when the direction of the potential on the reverse scan is switched at the foot of process II^{ox}. Other parameters are as in **a**

from the zero-current extrapolation method is 812 ± 13 mV.

A previous study [15] indicated that the peak current for the first reduction process varied linearly with scan rate only at scan rates below 200 mV/s. However, experimental data obtained in this study show that the linear region is a function of the amount of adhered C_{60}. Thus, a linear dependence on scan rate is observed for a scan rate < 200 mV/s for 20 μL of C_{60}/CH_2Cl_2, and < 100 mV/s and < 50 mV/s for 40 μL and 60 μL C_{60} dosages, respectively.

Effect of temperature

Table 2 summarizes the (E_f°) and ΔE_p dependence on temperature for the first couple when C_{60} was cast onto a 1 mm diameter gold electrode. The decrease in peak separation with increasing temperature implies the

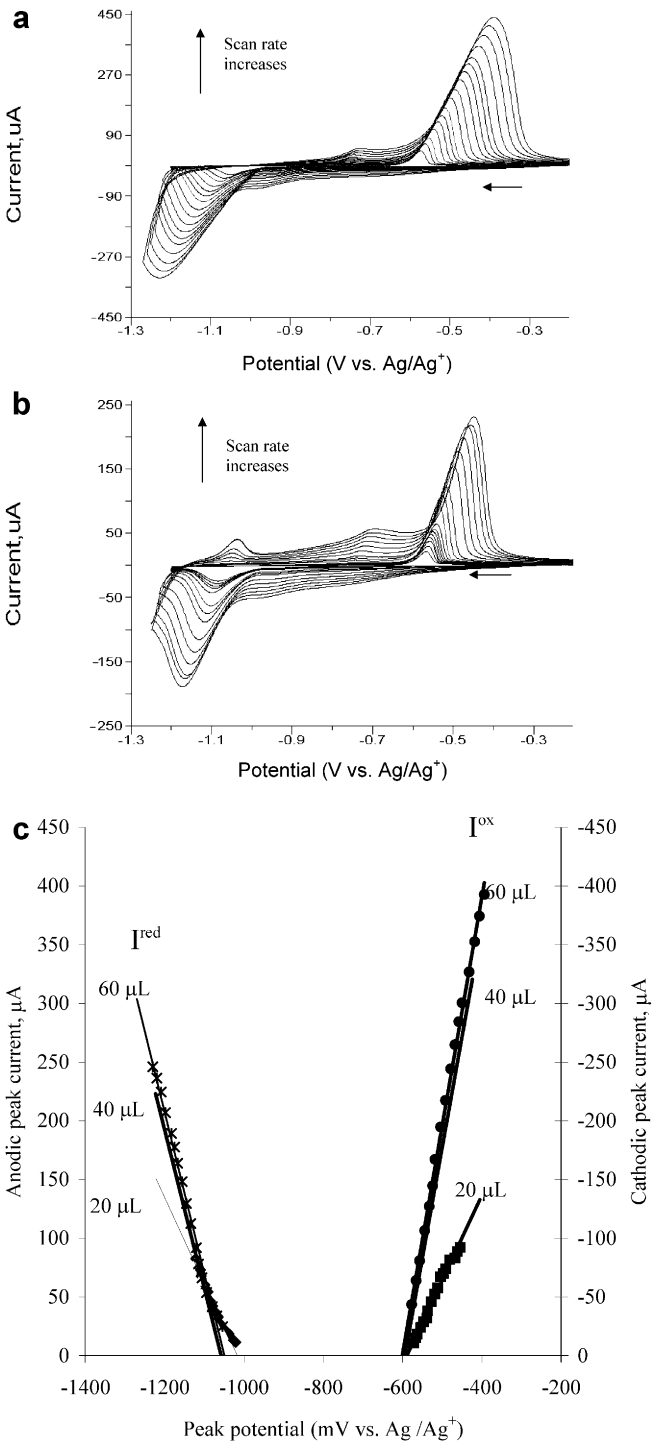

Fig. 4 **a** Cyclic voltammogram for 60 μL C_{60}/CH_2Cl_2 cast onto a 1 mm diameter gold electrode which is in contact with MeCN (0.1 M NBu_4PF_6) using scan rates of 10, 15, 20, 30, 40, 50, 60, 80, 100, 125, 150, 175, 200, 250, 300, 350 and 400 mV/s, with the third cycle being shown. **b** Cyclic voltammogram for microcrystalline C_{60} attached mechanically to a 1 mm diameter gold electrode which is in contact with MeCN (0.1 M NBu_4PF_6) using scan rates of 10, 15, 20, 30, 40, 50, 60, 80, 100, 150, 175, 200, 250, 300, 350 and 400 mV/s, with the second cycle being shown. **c** Plot of peak current versus peak potential for the $C_{60}^{0/-}$ process observed by varying the scan rate when different amounts of C_{60} are solvent cast onto a 1 mm gold electrode surface via the solvent casting method. The electrode was immersed in MeCN (0.1 M NBu_4PF_6)

Table 2 $\left(E_f^\circ\right)$ and ΔE_p values obtained for process I when 20 μL C_{60}/CH_2Cl_2 is coated onto a 1 mm gold electrode surface at specified temperatures. Other conditions are as in Fig. 1

Temperature (°C)	Peak separation, ΔE_p (mV)	Reversible potential, $\left(E_f^\circ\right)$ (mV)[a]
5	599	–822
15	579	–822
25	531	–816
35	497	–817
45	479	–816

[a]Calculated as $\left(E_p^{red} + E_p^{ox}\right)/2$

kinetics of the nucleation-growth rate-determining step increases with temperature, as expected.

Effect of varying the anion in the supporting electrolytes

The identity of the anion in a NBu_4^+ supporting electrolyte has very little influence on the potentials for the first two processes for the electroreduction of C_{60}, as shown by examination of the data in Table 3. This is consistent with results provided by Dubois et al. [29] and also, as predicted in Eqs. 1 and 2, represents a correct description of the processes.

Scanning electron microscopy

The main difference in electrode surface modification with C_{60} by solvent casting onto a 5 mm basal plane graphite electrode rather than direct mechanical attachment of microcrystals is that the solvent casting method produces a finer crop of more widely separated C_{60} microcrystalline particles. The SEM images in Fig. 5a reveal that particles of <2 μm are dominant when the solvent casting method is used, and also that a smooth film is not achieved with this method. One-electron reduced fulleride formed by controlled potential electrolysis for 60 s after the first reduction step in acetonitrile (0.1 M NBu_4PF_6) using solvent casting deposition generates significantly larger crystals than initially present. The size is further enhanced by an additional 60 s reduction (Fig. 5b). The second reduction step produces a set of even more

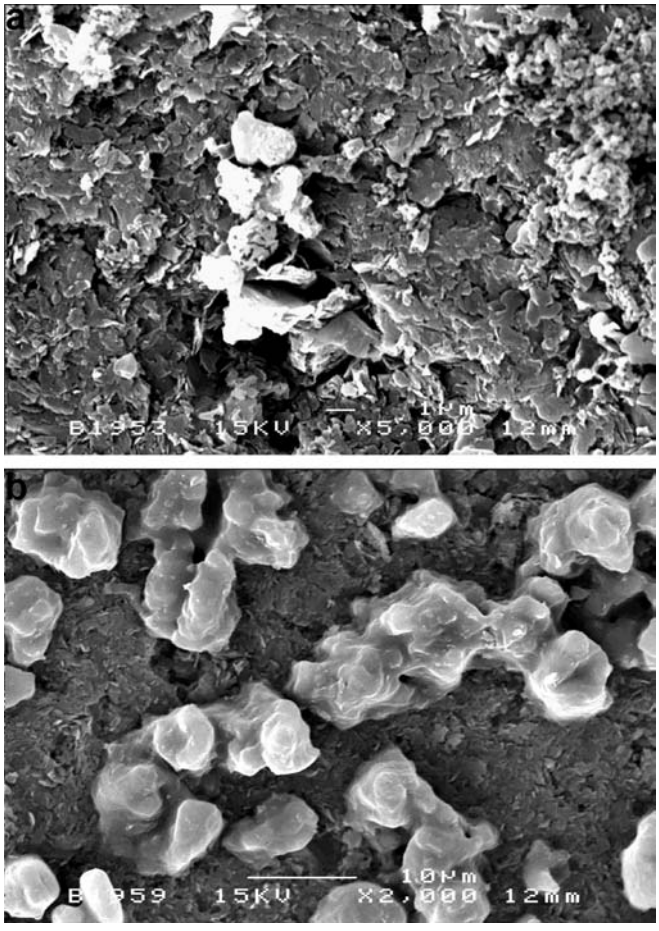

Fig. 5 **a** SEM image of C_{60} solvent cast onto a basal plane pyrolytic graphite electrode before electrolysis. **b** SEM image of C_{60} solvent cast onto a basal plane pyrolytic graphite electrode after holding the potential for 60 s at –1600 mV vs. Ag/Ag^+ in 0.1 M NBu_4PF_6/MeCN

sparsely distributed but larger microcrystals having an average size of about 5 μm (Fig. 5b). The rate at which enhancement of size occurs is greater using the solvent casting method, which implies that more effective electrolysis occurs than when commencing with mechanically attached microcrystals. It is also noted in Fig. 5b that the crystals have layers of solid particles growing on top of the base so that significant reconstruction of solid particles occurs on the electrode surface during the course of electrolysis, as also ap-

Table 3 Potential data obtained from the third voltammetric cycle of the potential (scan rate, 100 mV/s) when 20 μL C_{60}/CH_2Cl_2 was cast onto a 1 mm gold electrode which was then placed in contact with MeCN containing a 0.1 M concentration of a NBu_4^+ salt

Supporting electrolyte	Process I				Process II			
	E_p^{red} (mV)	E_p^{ox} (mV)	ΔE_p (mV)	$\left(E_f^\circ\right)$ (mV)[a]	E_p^{red} (mV)	E_p^{ox} (mV)	ΔE_p (mV)	$\left(E_f^\circ\right)$ (mV)[a]
NBu_4PF_6	–1081	–550	531	–816	–1300	–1050	250	–1168
NBu_4BF_4	–1102	–575	527	–839	–1334	–1056	278	–1195
NBu_4ClO_4	–1085	–554	531	–820	–1340	–1042	298	–1191
NBu_4Cl	–1095	–550	545	–823	–1340	–1030	310	–1185

[a]Calculated as $\left(E_p^{red} + E_p^{ox}\right)/2$

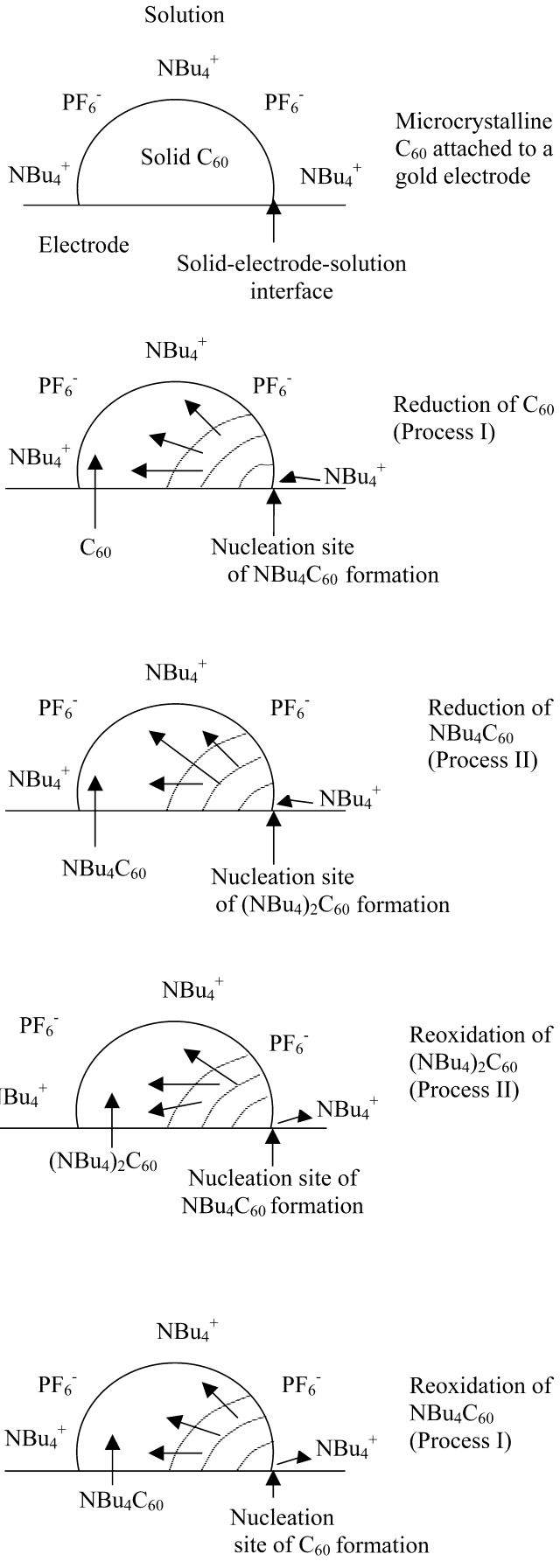

◄

Scheme 1 Schematic diagram of the nucleation processes believed to be associated with the electrochemical reduction of microcrystalline solid C_{60} and $(NBu_4)C_{60}$ and reoxidation of $(NBu_4)_2C_{60}$ and NBu_4C_{60} when the microcrystalline solid C_{60} is attached to an electrode and placed in contact with 0.1 M NBu_4PF_6/MeCN solution

pears to be the case with potential cycling experiments. The three-dimensional crystal growth and redistribution of solids have been detected in a previous study [13].

Discussion

Voltammetric studies on solvent cast and microcrstalline C_{60} fullerene mechanically adhered to an electrode surface immersed in acetonitrile containing 0.1 M NBu_4PF_6 electrolyte reveal that stable $C_{60}^{0/-}$ and $C_{60}^{-/2-}$ solid state transformation processes are achieved after three cycles of the potential. Detection of the presence of nucleation and growth processes has been obtained for both the $C_{60}^{0/-}$ and $C_{60}^{-/2-}$ couples. The linear dependence of peak current on dosage observed with the solvent casting deposition technique at low coverage implies that efficient electrolysis of the material is achieved. A zero-current extrapolation method produces peak potentials with values of –1032 mV and –588 mV vs. Ag/Ag^+ for the first reduction-reoxidation couple which are almost independent of the method of surface treatment or extent of surface coverage. Use of the SEM technique enabled the solid morphology to be observed before and after electrolysis and revealed that the solvent cast method produces smaller sized microcystals than those produced when direct mechanical attachment is employed. The electrolyzed products, irrespective of the initial origin of the microcystal, generate larger and more clearly defined crystalline features than those of initially adhered C_{60}, with crystals of $(NBu_4)_2C_{60}$ being slightly larger in size than $(NBu_4)C_{60}$.

In summary, evidence for a nucleation and growth process for the $C_{60}^{0/-}$ process provided by Suàrez et al. [13] is now extended to the $C_{60}^{-/2-}$ process for both the solvent cast and mechanically attached C_{60} crystals in the presence of acetonitrile/NBu_4^+ electrolyte. The basic concepts of the mechanism are illustrated in Scheme 1. The zero-current extrapolation method allows the determination of peak potentials which are almost independent of surface treatment, surface coverage and scan rate. The average of these values when a nucleation-growth process is rate determining can be assumed to represent a good approximation of the reversible potential for the processes given in Eqs. 1 and 2. Use of SEM enables subtle differences in the morphology of neutral C_{60} and electrolyzed C_{60} to be observed.

Acknowledgements The authors wish to thank Universiti Putra Malaysia and the Ministry of Science, Technology and Environment, Malaysia, for their financial support under the IRPA re-

search program (09-02-04-0051) and one of us (E.B.L.) for a graduate scholarship.

References

1. Haddon RC, Hebard AF, Rosseinsky MJ, Murphy DW, Duclos SJ, Lyons KB, Miller B, Rosamilla JM, Fleming RM, Kortan AR, Glarum SH, Makhija AV, Müller AJ, Eick RH, Zahurak SM, Tycko R, Dabbagh G, Thiel FA (1991) Nature 350:320
2. Hebard AF, Rosseinsky MJ, Haddon RC, Murphy DW, Glarum SH, Palstra TTM, Ramirez AP, Kortan AR (1991) Nature 350:600
3. Rosseinsky MJ, Ramirez AP, Glarum SH, Murphy DW, Haddon RC, Hebard AF, Palstra TTM, Kortan AR, Zahurak SM, Makhija AV (1991) Phys Rev Lett 66:2830
4. Stephens PW, Cox D, Lauher JW, Mihaly L, Wiley JB, Allemand PM, Hirsch A, Holczer K, Li Q, Thompson JD, Wudl F (1992) Nature 355:331
5. Allemand PM, Khemani KC, Koch A, Wudl F, Holczer K, Donovan S, Gruner G, Thompson JD (1991) Science 253:301
6. Miller B, Rosamilia JM, Dabbagh G, Tycko R, Haddon RC, Muller AJ, Wilson W, Murphy DW, Hebard AF (1991) J Am Chem Soc 113:6291
7. Winkler K, Costa DA, Balch AL, Fawcett WR (1995) J Phys Chem 99:17431
8. Fedurco M, Costa D, Balch AL, Fawcett WR (1995) Angew Chem Int Ed Engl 34:194
9. Allemand PM, Koch A, Wudl F, Rubin Y, Diederich F, Alvarez MM, Anz SJ, Whetten RL (1991) J Am Chem Soc 113:1051
10. Dubois D, Kadish KM, Flanagan S, Wilson LJ (1991) J Am Chem Soc 113:7773
11. Xie Q, Pérez-Cordero E, Echegoyen L (1992) J Am Chem Soc 114:3978
12. Ohsawa Y, Saji T (1992) J Chem Soc Chem Commun 781
13. Suàrez MF, Marken F, Compton RG, Bond AM, Miao W, Raston CL (1999) J Phys Chem B 103:5637
14. Jehoulet C, Bard AJ, Wudl F (1991) J Am Chem Soc 113:5456
15. Jehoulet C, Obeng YS, Kim YT, Zhou F, Bard AJ (1992) J Am Chem Soc 114:4237
16. Compton RG, Spackman RA, Wellington RG, Green MLH, Turner J (1992) J Electroanal Chem 327:337
17. Compton RG, Spackman RA, Riley DJ, Wellington RG, Eklund JC, Fisher AC, Green MLH, Doothwaite RE, Stephens AHH, Turner J (1993) J Electroanal Chem 344:235
18. Oyama N, Tatsuma T, Kikuyama S (1994) J Electroanal Chem 379:523
19. Balch AL, Costa DA, Fawcett WR, Winkler K (1997) J Electroanal Chem 427:137
20. Winkler K, Costa DA, Balch AL, Fawcett WR (1998) J Electroanal Chem 456:229
21. Carlisle JJ, Wijayawardhana CA, Evans TA, Melaragno PR, Ailin-Pyzik IB (1996) J Phys Chem 100:15532
22. Koh W, Dubois D, Kutner W, Jones MT, Kadish KM (1993) J Phys Chem 97:6871
23. Cheng F-X, Li N-Q, He W-J, Gu Z-N, Zhou X-H, Sun Y-L, Wu Y-Q (1996) J Electroanal Chem 408:101
24. Nishizawa M, Tomura K, Matsue T, Uchida I (1994) J Electroanal Chem 379:233
25. Koh W, Dubois D, Kutner W, Jones MT, Kadish KM (1992) J Phys Chem 96:4163
26. Zhaou F, Yao S-L, Jehoulet C, Laude DA Jr, Guan Z, Bard AJ (1992) J Phys Chem 96:4160
27. Fletcher S, Halliday CS, Gates D, Westcott M, Lwin T, Nelson G (1983) J Electroanal Chem 159:267
28. Shaw SJ, Marken F, Bond AM (1996) Electroanalysis 8:732
29. Dubois D, Gilles M, Kutner W, Jones MT, Kadish KM (1992) J Phys Chem 96:7137